

Quasinormal modes and late-time falloff of Finslerian black holes with cosmological constant

Tian-Yang Li,^{*} Su-Ping Zhao,[†] and Xin Li[‡]

*Department of Physics and Chongqing Key Laboratory for Strongly Coupled Physics,
Chongqing University, Chongqing 401331, China*

 (Received 5 June 2021; revised 15 February 2022; accepted 5 May 2022; published 20 May 2022)

Quasinormal modes of scalar and electromagnetic field perturbations in Finslerian Reissner-Nordström black holes with a cosmological constant are investigated in this paper. We analyze the fundamental frequencies and dynamical evolution of quasinormal modes using the WKB approximation and finite difference method, respectively. Both approaches show that the periods of oscillation of quasinormal modes increase with higher Finslerian parameter ϵ^2 if the multipole quantum number $l \geq 2$. Using the Prony method, we show that the results obtained from the finite difference method are consistent with the results obtained from the WKB approximation. Quasinormal modes of Finslerian black holes possess spectrum splitting, which reflects the fact that the spherical symmetry of the Finslerian black holes is broken. The effects of the Finslerian parameter ϵ^2 on the late-time tails of scalar and electromagnetic field perturbations are shown. The late-time tails of the Finslerian Reissner-Nordström black holes possess a power-law falloff. The power-law index has a discontinuous jump, while the Finslerian parameter ϵ^2 varies from 0 to nonzero. Such a fact reflects the fact that asymptotic-infinity behaviors of the Finslerian Reissner-Nordström black holes are different from their counterparts in general relativity.

DOI: [10.1103/PhysRevD.105.104042](https://doi.org/10.1103/PhysRevD.105.104042)

I. INTRODUCTION

The black hole, as a region with strong gravity, has been widely discussed by physicists. In general relativity, the Schwarzschild solution has predicated the existence of black holes. Penrose gave a robust proof that black holes can be formed without the assumption of high symmetry [1]. Black holes can be generated through three ways, namely, the gravitational collapse of a heavy star [2], the gravitational collapse of a primordial overdensity in the early Universe [3–5], or high energy collisions [6].

Accretion disks [7], as a typical astronomical phenomena, can be used to locate supermassive black holes located at the centers of galaxies. Observations of a hot accretion flow for Sagittarius A* have shown that it is a candidate for a supermassive black hole [8]. The orbits of several stars around Sagittarius A* have been precisely observed by the GRAVITY Collaboration [9]. This also confirms that Sagittarius A* is compatible with black holes predicted by general relativity. The first released picture of the centre of M87 by the Event Horizon Telescope Collaboration has shown the existence of a supermassive compact object at the centre of M87 [10]. A detailed analysis of the shadow of

this picture provides strong support for the fact that such a supermassive object is a supermassive black hole.

The above progress has shown universal existence of the black holes in our cosmology from both theoretical and experimental researches. On behalf of the detection of gravitational waves [11], properties of black holes can be investigated from direct gravitational effect. The ongoing third generation of gravitational-wave detectors, such as the Einstein Telescope [12], will provide more precise observations of binary black holes mergers. Though general relativity has been tested by various observations with high precision [13], the observation of gravitational waves could become a powerful tool to test general relativity in strong gravitational region.

To study possible quantum effects of gravity or to search for possible explanations of dark energy or dark matter, various modified theories of gravity have been proposed [14], such as $f(R)$ gravity [15], $f(R, T)$ gravity [16], and Bekenstein's TEVES theory [17]. The modified theories of gravity mentioned above share one common feature, namely, the background geometry, which is Riemannian. Finsler geometry [18] is a natural generalization of Riemannian geometry. It is expected that a gravitational theory based on Finsler geometry will provide different gravitational effects than other modified theories of gravity. Based on the geodesic deviation equation, Rutz suggested that the Finslerian vacuum gravitational field equation is vanishing of the Ricci scalar [19]. We have derived exact

^{*}litianyang@cqu.edu.cn

[†]zhaosp@cqu.edu.cn

[‡]lixin1981@cqu.edu.cn

solutions from Rutz's field equation. These solutions admit the existence of Finslerian black holes, namely, Finslerian Schwarzschild black holes [20] and Finslerian Reissner-Nordström black holes [21]. The Finslerian black holes derived by us preserve a special symmetry. It is a warp product spacetime and its two-dimensional subspace is Finsler space with constant curvature. In Ref. [22], general existences of Finslerian black holes have been proved. As a counterpart of Penrose's singularity theorem [1], Jacobi fields and the Ricci scalar play an important role in their proofs [22]. The above facts imply that Rutz's field equation [19] could be a reasonable Finslerian gravitational field equation.

Though the mathematical existence of Finslerian black holes has been established, the physical existence of Finslerian black holes in cosmology should be tested by astronomical experiments. Quasinormal modes (QNMs), generated by perturbations of black holes, carry intrinsic information of black holes. Thus, QNMs have been discussed intensively by physicists to test various modified theories of gravity [23–30]. The frequencies of QNMs are a characteristic property of the ringdown phase, which is the last process of merge of binary. Up to now, three types of binary mergers—binary black hole, binary neutron star, and neutron star–black hole mergers—have been detected [11,31]. Ongoing third-generation gravitational-wave detectors (such as the Einstein Telescope [12]) and space-borne detectors (such as LISA [32] and Taiji [33]) will provide more precise observations and a broad detection frequency band of the ringdown phase. Therefore, it is interesting and important to test Finslerian black holes using QNMs.

We have investigated QNMs of specific Finslerian Schwarzschild black holes [34]. Current cosmological observations show that our Universe is undergoing accelerated expansion, which implies the existence of a cosmological constant [35]. Thus, the effect of a cosmological constant should be considered in investigating the QNMs of Finslerian black holes. In this paper, we study the QNMs of Finslerian Reissner-Nordström black holes with a cosmological constant. In Finsler geometry, spaces with constant curvature are not equivalent [21]. Therefore, Finslerian Schwarzschild spacetime [20] and Finslerian Reissner-Nordström spacetime [21] cannot be uniquely determined by Rutz's Finslerian gravitational field equation [19]. Rutz's field equation can be regarded as an extension of Einstein's field equation. The above fact implies that other constraints are needed to determine the gravitational properties of Finsler spacetime. The asymptotic-infinity behaviors of all Finslerian Schwarzschild solutions, including the Schwarzschild solution, are different. Late-time tails of perturbations of black holes reflect the asymptotic-infinity behaviors of black holes [36]. Thus, research on the late-time tail of perturbations of Finslerian black holes may shed light on obtaining the hidden constraints on Finsler spacetime.

This paper is organized as follows. In Sec. II we briefly introduce the Finslerian Reissner-Nordström black holes. Using the Finslerian Laplace operator and the divergence operator, the equations of motion of a scalar field and electromagnetic field can be derived. In Sec. III we use the finite difference method, WKB approximation, and Prony method to analyze the dynamic evolution and frequencies of QNMs, respectively. The late-time tails are discussed in this section. Finally, discussions and conclusions are presented in Sec. IV.

II. QUASINORMAL MODES IN FINSLERIAN-REISSNER-NORDSTRÖM SPACETIME

A. Finslerian Reissner-Nordström black holes

The basic geometric quantity of Finsler geometry is the Finsler structure F [18]. The arc length of Finsler geometry is defined as $L(\tau) = \int F(x(\tau), y(\tau)) d\tau$, where x denotes the coordinate of the Finsler manifold M and $y \in T_x M$. The Finsler structure satisfies the property $F(x, \lambda y) = \lambda F(x, y)$, $\lambda > 0$. This property guarantees that the Finsler structure is well defined, namely, that the arc length is independent of the choice of the parameter τ . The Finslerian metric is given as

$$g_{\mu\nu} \equiv \frac{\partial}{\partial y^\mu} \frac{\partial}{\partial y^\nu} \left(\frac{1}{2} F^2 \right). \quad (1)$$

In Ref. [18] the Finsler structure was taken to be positive definite. However, in physics the Finsler structure F is not positive definite at every point of the Finsler manifold. The causal structure of Finsler spacetime directly depends on the sign of F^2 [22,37].

In our previous research [21], a specific Finslerian Reissner-Nordström (RN) solution was obtained from Rutz's Finslerian gravitational field equation [19], which is distinguishing with the Reissner-Nordström solution only in two-dimensional subspace. It is given as

$$F^2 = -f(r)y^t y^t + f(r)^{-1} y^r y^r + r^2 \bar{F}^2, \quad (2)$$

where $f(r) = 1 - \frac{2GM}{r} - br^2 + \frac{q^2}{r^2}$, M and $q^2 = 4\pi GQ^2$ are the mass and charge of the black hole, respectively, and b is a cosmological constant. \bar{F} is a two-dimensional Finsler space with positive constant flag curvature. One of the major differences between Riemannian geometry and Finsler geometry is that Finsler spaces with constant flag curvature are not equivalent to each other. For example, the Finsler space derived by Byrant [38] is not equivalent to the one derived by Shen [39]. Different choices of nonequivalent Finsler spaces with constant flag curvature could response on the different behaviors of QNMs, namely, the frequencies and their late-time falloff. This is because of the difference black hole geometry. In this paper, in order to be consistent with our former results on QNMs in

Finslerian Schwarzschild black holes [34], we only consider a Finsler space \bar{F} with the following form [20,39]:

$$\bar{F} = \frac{\sqrt{(1 - \epsilon^2 \sin^2 \theta) y^\theta y^\theta + \sin^2 \theta y^\varphi y^\varphi}}{1 - \epsilon^2 \sin^2 \theta} - \frac{\epsilon \sin^2 \theta y^\varphi}{1 - \epsilon^2 \sin^2 \theta}, \quad (3)$$

where ϵ is the Finslerian parameter, and $0 \leq \epsilon < 1$. The Finsler space \bar{F} [Eq. (3)] is an extension of Riemannian sphere.

QNMs have already been studied in Finslerian Schwarzschild spacetime with the two-dimensional subspace \bar{F} . Together with the following study on QNMs of Finslerian RN black holes, we obtain more perturbational properties of Finslerian black holes with the two-dimensional subspace \bar{F} .

B. Scalar field and electromagnetic field perturbations of Finslerian RN black holes

In general relativity, electromagnetic field perturbations of RN black holes with a cosmological constant are related to gravitational perturbations of black holes [40,41]. Gravitational perturbations of Finslerian black holes will involve detailed analysis on Finslerian gravitational field equation. This is beyond the scope of this paper and will be considered in the future. Therefore, in this paper we only consider the scalar and electromagnetic field perturbations of Finslerian RN black holes [Eq. (2)]. The energy-momentum tensor of scalar and electromagnetic field perturbations is quadratic in the scalar and electromagnetic fields. Therefore, in the linear approximation, these perturbed fields do not contribute to the gravitational field equation, i.e., the background Finslerian RN black holes (2) are unaffected by the perturbations. This implies that scalar and electromagnetic field perturbations satisfy the Klein-Gordon and Maxwell equations in the Finsler spacetime (2), respectively. These equations are related to the Laplace operator and divergence operator in Finsler geometry. It should be mentioned that several different ways of definition of Finslerian are not equivalent. In this paper we use the Finslerian Laplace operator defined in Refs. [42,43] that was used in our former research [34]. It makes the results of QNMs in Finslerian RN black holes comparable and consistent with the results of QNMs in Finslerian Schwarzschild black holes [34].

For any one-form $A = A_\mu dx^\mu$ and smooth function ϕ , the Finslerian Laplace operator and divergence operator [43] are given as

$$\Delta \phi = \sigma^{-1} \partial_\mu (\bar{g}^{\mu\nu} \sigma \partial_\nu \phi), \quad (4)$$

$$\text{div} A = \sigma^{-1} \partial_\mu (\bar{g}^{\mu\nu} \sigma \partial_\nu A_\nu), \quad (5)$$

where σ denotes the Holmes-Thompson volume element in Finsler geometry [44]. $\bar{g}^{\mu\nu}$ is defined in terms of the Finsler metric $g^{\mu\nu}$,

$$\bar{g}^{\mu\nu} = \sigma^{-1} c_{n-1}^{-1} \int_{S_x M} g^{\mu\nu} \det(g_{\mu\nu}/F) d\eta, \quad (6)$$

where c_{n-1} denotes the volume of the unit Euclidean $(n-1)$ -sphere, $S_x M = \{y \in T_x M | F(y) = 1\}$, and

$$d\eta = \sum_{i=1}^n (-1)^{i-1} y^i dy^1 \wedge \cdots \wedge \widehat{dy^i} \wedge \cdots \wedge dy^n. \quad (7)$$

The Holmes-Thompson volume element is given as

$$\sigma = c_{n-1}^{-1} \int_{S_x M} \det(g_{\mu\nu}/F) d\eta. \quad (8)$$

It should be noticed that $\bar{g}^{\mu\nu}$ is the Riemannian metric. Thus, the Finslerian Laplace operator defined in Refs. [42,43,45] is a weighted Riemannian Laplace operator. Although the Finslerian Laplace operator and divergence operator are very similar to the Riemannian one, it still carries important information about Finsler spacetime, such as the Holmes-Thompson volume element σ , and the Riemannian metric $\bar{g}^{\mu\nu}$ can be regarded as an average of the Finsler metric $g^{\mu\nu}$.

The Finslerian RN black holes (2) and the Finslerian Schwarzschild black holes [20] both possess the same two-dimensional subspace \bar{F} (3). Therefore, following the same approach used in Ref. [34] and after some tedious calculations, we obtain that the radial and time components of the scalar field and electromagnetic field perturbations satisfy the following Schrödinger-like equation:

$$-\frac{\partial^2 R}{\partial t^2} + \frac{\partial^2 R}{\partial r_*^2} = VR, \quad (9)$$

where $dr_* = dr/f$ is the tortoise coordinate. In Eq. (9), the effective potential V of scalar field perturbations, axial mode and polar mode of electromagnetic field perturbations are given as

$$V^S = f \left(\frac{\lambda^S}{r^2} + \frac{1}{r} \frac{df}{dr} \right), \quad (10)$$

$$V^A = \frac{f \lambda^A}{r^2}, \quad (11)$$

$$V^P = \frac{f \lambda^S}{r^2}, \quad (12)$$

respectively. The parameters $-\lambda$ in the above formulas denote the eigenvalues of modified spherical harmonics derived from the equation of motion of scalar field perturbations and the axial and polar modes of electromagnetic field perturbations, respectively. These eigenvalues are given as

$$\lambda^S = l(l+1) - \epsilon^2 \left(\frac{3(l-1)l(l+1)(l+2)}{2(2l-1)(2l+3)} + \frac{m^2(7l^2+7l+6)}{2(2l-1)(2l+3)} \right), \quad (13)$$

$$\lambda^A = l(l+1) - \epsilon^2 \left(\frac{l(l+1)(3l^2+3l-2)}{2(2l-1)(2l+3)} + \frac{m^2(7l^2+7l-6)}{2(2l-1)(2l+3)} \right), \quad (14)$$

where l and m denote the multipole quantum number and magnetic quantum number of spherical harmonics, respectively.

It should be noticed that different choices for the Finslerian Laplace operator alter the solutions of the angular part for perturbed field. The properties of the QNMs of black holes only depend on the radial and time components of field perturbations. Different choices for the Finslerian Laplace operator correspond to different eigenvalues of the solutions of the angular part for a perturbed field, and different eigenvalues could alter the frequencies of QNMs and the power-law index of the late-time tails.

III. NUMERICAL RESULTS

A. Dynamical evaluation of QNMs

In this paper we use the finite difference method [46] with a second-order scheme to investigate the dynamical evaluation of QNMs in a specific Finslerian RN black hole. Introducing the light-cone coordinates $\mu = t - r_*$ and $\nu = t + r_*$, the Schrödinger-like equation (9) can be simplified as

$$\left(4 \frac{\partial^2}{\partial \mu \partial \nu} + V(\mu, \nu) \right) R(\mu, \nu) = 0. \quad (15)$$

Using a grid cell scale $h = \delta\mu = \delta\nu$, Eq. (15) can be discretized through Taylor expansion as

$$R(\mu + \delta\mu, \nu + \delta\nu) = R(\mu, \nu + \delta\nu) + R(\mu + \delta\mu, \nu) - R(\mu, \nu) - \Delta\mu\Delta\nu \left(\frac{2\nu - 2\mu + \delta\nu - \delta\mu}{4} \right) \frac{R(\mu + \delta\mu, \nu) + R(\mu, \nu + \delta\nu)}{8} + \mathcal{O}(h^4). \quad (16)$$

The boundary condition applied in the calculation is $R(\mu, \nu = 0) = 0$, and the initial condition is a Gaussian pulse $R(\mu = 0, \nu) = \exp[-(\nu - \nu_c)^2/2\omega^2]$. Additionally, we set the grid cell scale $h = 0.5$ and obtain the dynamical evaluations of QNMs at a fixed $r_* = 0$.

To find the independent influences of the charge q and cosmological constant b on QNMs frequencies, we first

consider the two cases, i.e., Finslerian RN black holes and Finslerian Schwarzschild–de Sitter (SdS) black holes, respectively. Then, the impacts of the joint action of the two parameters are considered for Finslerian RN–de Sitter (RNdS) black holes. Our results for these conditions at $\epsilon^2 = 0$ are consistent with the calculations in general relativity [41,47]. The dynamic evolutions of the QNMs

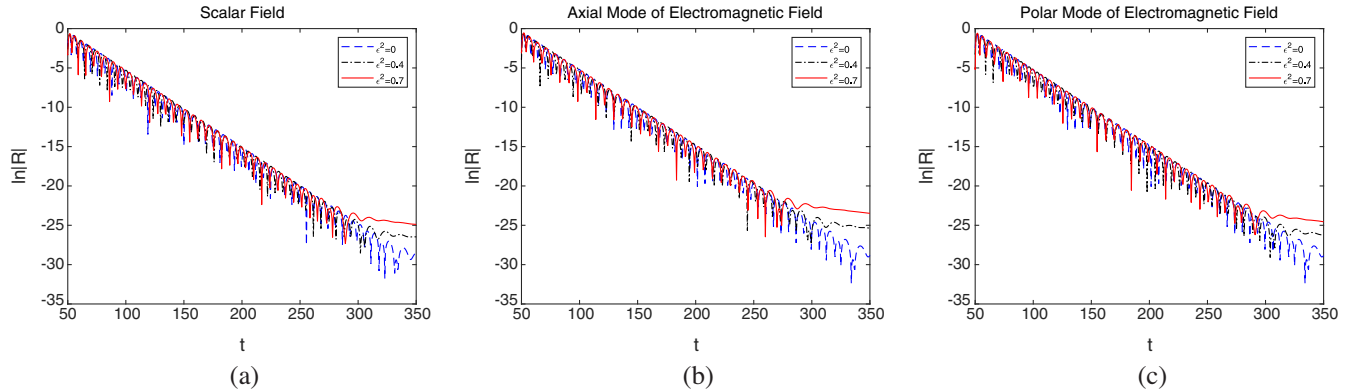


FIG. 1. Dynamical evolution of the QNMs of scalar and electromagnetic field perturbations in Finslerian RN black holes with various ϵ^2 . The parameters used are $q = 0.5$, $l = 2$, and $m = 0$. The parameters of the Gaussian pulse are $\nu_c = 50$ and $\omega = 1.414$.

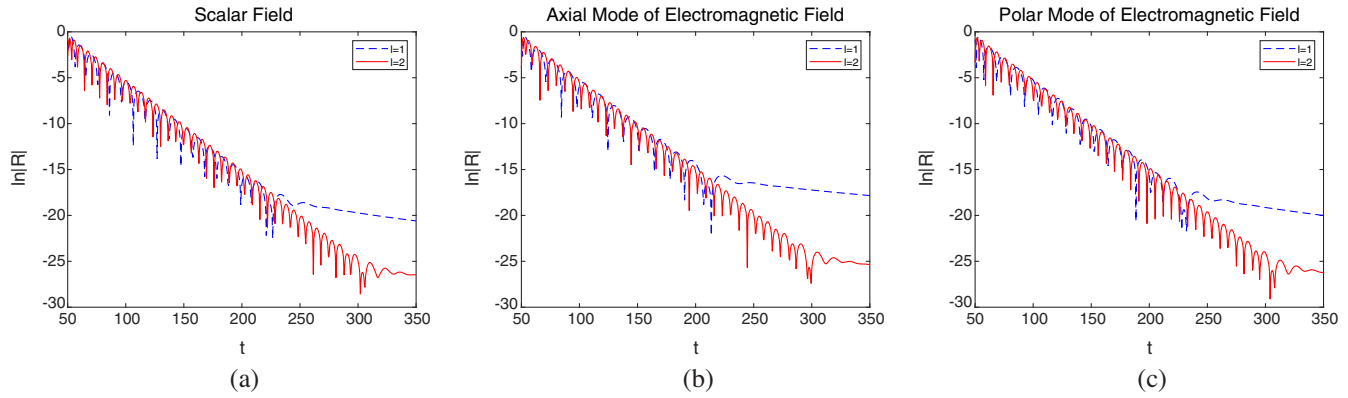


FIG. 2. Dynamical evolution of the QNMs of scalar and electromagnetic field perturbations in Finslerian RN black holes with various l . The parameters used are $q = 0.5$, $\epsilon^2 = 0.4$, and $m = 0$. The parameters of the Gaussian pulse are $\nu_c = 50$ and $\omega = 1.414$.

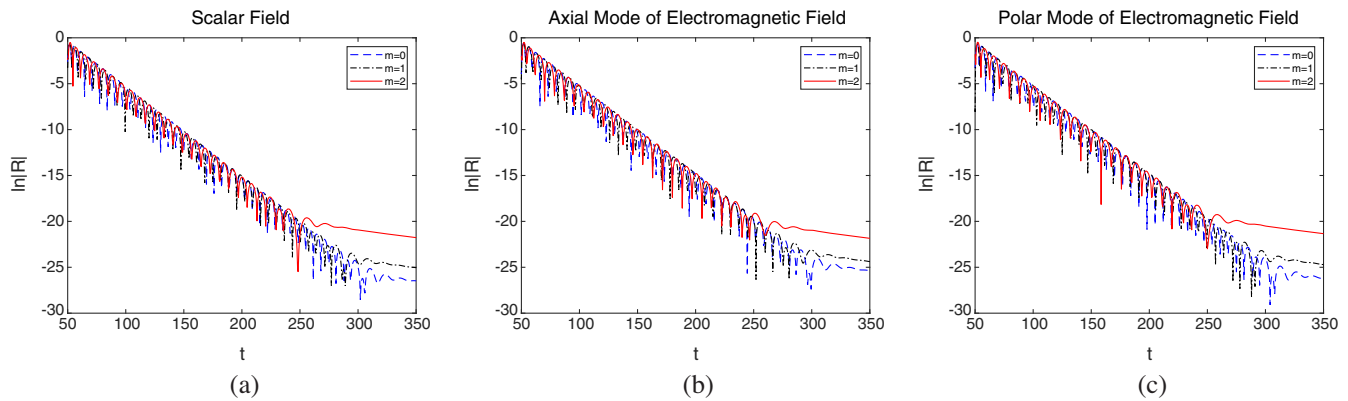


FIG. 3. Dynamical evolution of the QNMs of scalar and electromagnetic field perturbations in Finslerian RN black holes with various m . The parameters used are $q = 0.5$, $l = 2$, and $\epsilon^2 = 0.4$. The parameters of the Gaussian pulse are $\nu_c = 50$ and $\omega = 1.414$.

of Finslerian RN black holes are shown in Figs. 1–3. These figures show that the periods of oscillation for scalar and electromagnetic field perturbations both increase with higher ϵ^2 and m , and decrease with lower l . However, the decay rates of the peak of the dynamical evolution of

QNMs are less affected by varying the parameters (l , ϵ^2 and m). The periods of oscillation are inversely proportional to the real part of the complex frequencies.

Next, we consider the impacts of the parameters (ϵ^2 , l , and m) on the Finslerian SdS black holes. The results are

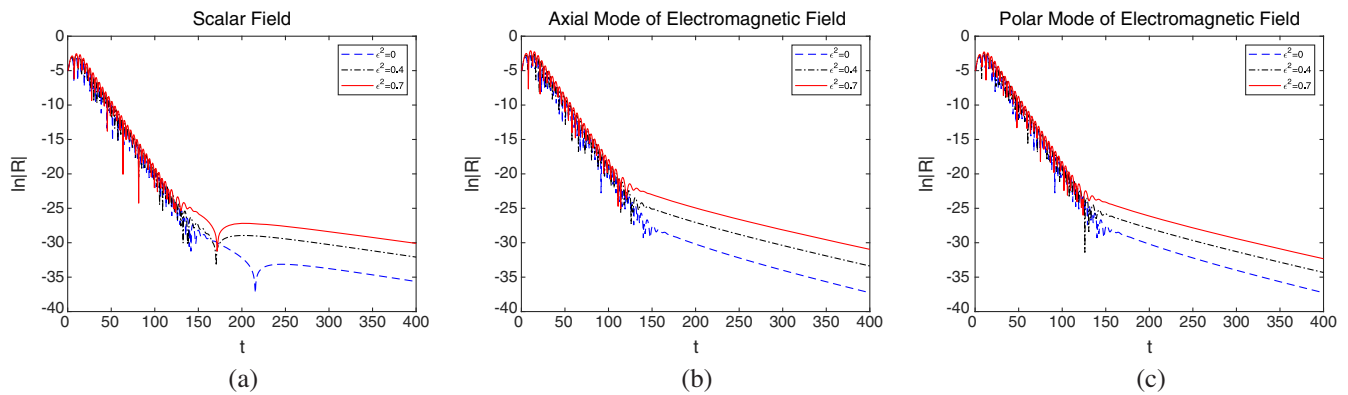


FIG. 4. Dynamical evolution of the QNMs of scalar and electromagnetic field perturbations in Finslerian SdS black holes with various ϵ^2 . The parameters used are $l = 2$ and $m = 0$, and the event horizon and cosmological horizon are $r_e = 1$ and $r_c = 100$, respectively. The parameters of the Gaussian pulse are $\nu_c = 10$ and $\omega = 3$.

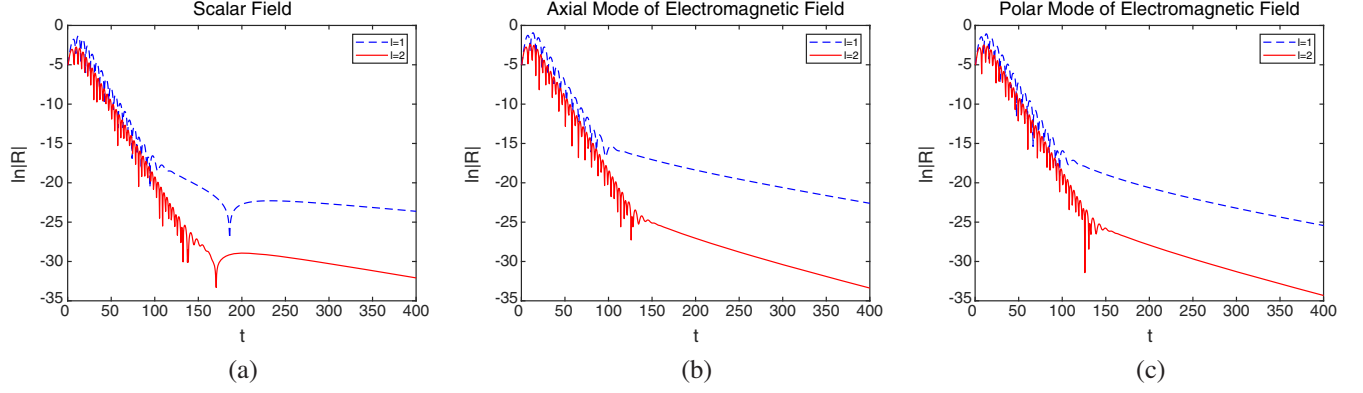


FIG. 5. Dynamical evolution of the QNMs of scalar and electromagnetic field perturbations in Finslerian SdS black holes with various l . The parameters used are $\epsilon^2 = 0.4$ and $m = 0$, and the event horizon and cosmological horizon are $r_e = 1$ and $r_c = 100$, respectively. The parameters of the Gaussian pulse are $\nu_c = 10$ and $\omega = 3$.

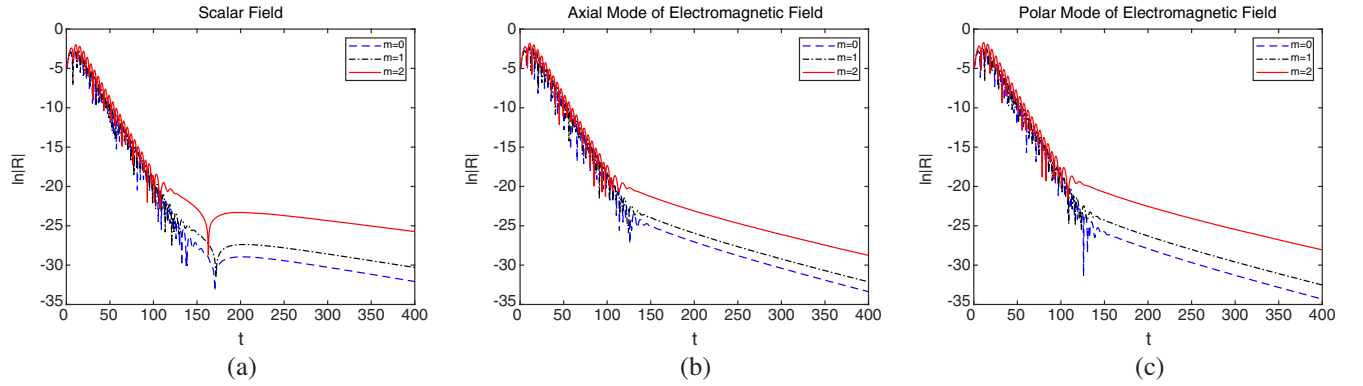


FIG. 6. Dynamical evolution of the QNMs of scalar and electromagnetic field perturbations in Finslerian SdS black holes with various m . The parameters we used are $\epsilon^2 = 0.4$ and $l = 2$, and the event horizon and cosmological horizon are $r_e = 1$ and $r_c = 100$, respectively. The parameters of the Gaussian pulse are $\nu_c = 10$ and $\omega = 3$.

plotted in Figs. 4–6, respectively. One should notice that a long oscillation will appear at $t \lesssim r_c/c$ with scalar field perturbations for Finslerian SdS black holes and Finslerian RNdS black holes. This means that an exponential decay

replaces the power-law decay, which is a special phenomenon with a small positive cosmological constant [47].

Finally, we consider the dynamical evolution of the QNMs of the Finslerian RNdS black holes. Here we only

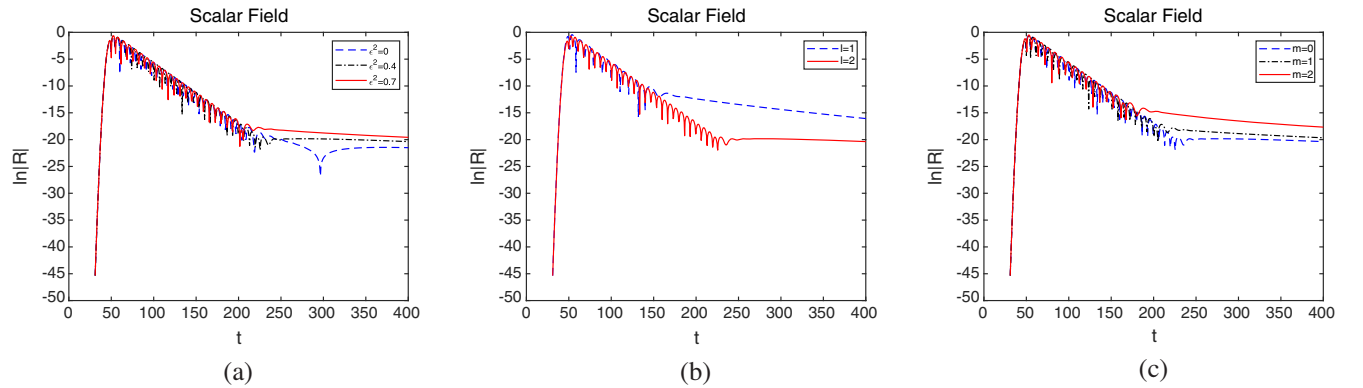


FIG. 7. Dynamical evolution of the QNMs of scalar perturbations in Finslerian RNdS black holes with various ϵ^2 , l , and m , respectively. The common parameters used are $b = 10^{-5}$ and $q = 0.5$. The specific parameters are $l = 2$ and $m = 0$ for panel (a), $\epsilon^2 = 0.4$ and $m = 0$ for panel (b), and $l = 2$ and $\epsilon^2 = 0.4$ for panel (c). The parameters of the Gaussian pulse are $\nu_c = 50$ and $\omega = 2$.

consider scalar field perturbations in Finslerian RNdS black holes since the electromagnetic and gravitational modes are coupled. The parameters of the Gaussian pulse ain calculating the Finslerian RNdS black hole are the same as for the Finslerian SdS black holes. The impacts of the three parameters (ϵ^2 , l , and m) on the dynamical evolution are shown in Fig. 7.

B. Frequencies of QNMs

1. WKB approximation

In this section we use the WKB approximation [48] to obtain the frequencies of QNMs from the Schrödinger-like equation (9). To improve the accuracy of the characteristic frequencies of QNMs, the higher-order WKB approach was derived by Iyer and Will [49] and Konoplya [50]. In this paper, the sixth-order WKB approximation is utilized to obtain the frequencies of QNMs, and it is of the form

$$\frac{i(\omega^2 - V_0)}{\sqrt{-2V_0''}} \Big|_{r=r_0} = n + \frac{1}{2} + \sum_{i=2}^6 \Lambda_i, \quad (n = 0, 1, 2, \dots), \quad (17)$$

where V_0 is the maximum potential at $r = r_0$ and Λ_i are the i th-order correction terms, whose specific forms can be found in Refs. [48–50]. Fundamental QNMs frequencies labeled by overtone number $n = 0$ are the least damped mode [24] that usually dominates the ringdown waveform and more likely to be detected in the ongoing third generation of gravitational wave detectors. Thus, we only study the fundamental QNM frequencies of Finslerian black holes in this paper. The convergence of the sixth-order WKB approximation was discussed in Ref. [25], where it was shown that in many cases, when $n \leq l$, the sixth-order WKB approximation gives better results. In this paper we only consider fundamental QNM frequencies, which means that $n \leq l$ and the sixth-order WKB approximation is suitable.

Meanwhile, the effective potential of the Finslerian RN anti-de Sitter black holes has no extremum and is not convergent at infinity. Its complex frequencies cannot be obtained with the WKB approximation. Therefore, in this paper we only consider three special cases of QNMs of Finslerian RN black holes with a cosmological constant [Eq. (2)], i.e., QNMs of the Finslerian RN black holes ($b = 0$), QNMs of Finslerian SdS black holes ($q = 0$), and QNMs of scalar field perturbations of Finslerian RNdS black holes ($b > 0$). In these cases of a probe electromagnetic field, the spacetime is fixed and does not evolve.

For the three special cases of Finslerian RN black holes with a cosmological constant, we discuss the influence of the three parameters on QNMs frequencies, namely, the Finslerian parameter ϵ^2 , multipole quantum number l , and magnetic quantum number m . In this paper, without loss of

generality, we set the parameter $GM = 1$ to obtain numerical results for Finslerian RN black holes and Finslerian RNdS black holes. To compare our results with QNMs of SdS black holes in general relativity [47], we consider an event horizon r_e and cosmological horizon r_c in calculating the QNMs of Finslerian SdS black holes. These parameters possess the following relations with metric components $f(r)$ and b and GM :

$$f = 1 - \frac{2GM}{r} - br^2 = b \left(1 - \frac{r_e}{r} \right) (r_c - r)(r + r_e + r_c), \quad (18)$$

$$b = (r_e^2 + r_e r_c + r_c^2)^{-1}, \quad (19)$$

$$GM = \frac{br_e r_c (r_e + r_c)}{2}. \quad (20)$$

The Finslerian parameter ϵ^2 in the Finslerian black holes (2)–(3) plays an important role in depicting the deviation from black holes in general relativity. Thus, we focus on investigating the impact of ϵ^2 on the complex frequencies of the QNMs of Finslerian black holes. The numerical results are listed in Tables I–III. It should be noticed that the Finslerian parameter ϵ^2 does not affect the QNM spectrum when $l = 0$ for the scalar field perturbations and $l = 1 (m = 0)$ for polar modes of electromagnetic field perturbations. There are also clear changes in the QNMs when $(l, m) = (1, 0)$ between the axial and polar modes of electromagnetic field perturbations. This is due to the fact that the nonvanishing ϵ^2 breaks spherical symmetry. The three special cases of Finslerian RN black holes with a cosmological constant have similar behaviors for the field perturbations. For scalar field perturbations, the magnitude of $\text{Re}(\omega_0)$ decreases with higher ϵ^2 , while the magnitude of $|\text{Im}(\omega_0)|$ increases with higher ϵ^2 . For axial and polar modes of electromagnetic field perturbations, the magnitudes of $\text{Re}(\omega_0)$ and $|\text{Im}(\omega_0)|$ both decrease with higher ϵ^2 . The Finslerian effect on the QNMs can be attributed to the eigenvalues of the modified spherical harmonics [Eqs. (13)–(14)]. The eigenvalue λ can be written in terms of the effective multipole quantum number ν , namely, $\lambda \equiv \nu(\nu + 1)$. In many cases, the effective multipole quantum number ν decreases with higher ϵ or m . Therefore, these results are obvious from the properties of the quasinormal frequencies of RN black holes. It should be noticed that the eigenvalues (13)–(14) both return to that in general relativity when $\epsilon^2 = 0$ or $l = 0$. This means that the QNM frequencies of Finslerian black holes will also return to that in general relativity when $\epsilon^2 = 0$ or $l = 0$. Under such special conditions, we find that our numerical results are consistent with the results in general relativity [51–53].

The two-dimensional subspace of Finslerian black holes (3) breaks spherical symmetry. Such fact responses to the

TABLE I. Fundamental QNM frequencies for scalar and electromagnetic field perturbations with various l and ϵ^2 in Finslerian RN black holes. The values are calculated using the sixth-order WKB approximation, and the parameters used in the calculation are $m = 0$ and $q = 0.5$.

l	ϵ^2	Electromagnetic					
		Scalar		Axial		Polar	
		$\text{Re}(\omega_0)$	$\text{Im}(\omega_0)$	$\text{Re}(\omega_0)$	$\text{Im}(\omega_0)$	$\text{Re}(\omega_0)$	$\text{Im}(\omega_0)$
0	0.1	0.115747	-0.1019980
1	0.1	0.306551	-0.0988743	0.255082	-0.0939979	0.261322	-0.0941246
	0.2	0.306551	-0.0988743	0.248689	-0.0938613	0.261322	-0.0941246
	0.3	0.306551	-0.0988743	0.242130	-0.0937140	0.261322	-0.0941246
	0.4	0.306551	-0.0988743	0.235392	-0.0935550	0.261322	-0.0941246
	0.5	0.306551	-0.0988743	0.228460	-0.0933823	0.261322	-0.0941246
2	0.1	0.499056	-0.0979638	0.469852	-0.0962429	0.472307	-0.0962544
	0.2	0.492048	-0.0979792	0.459900	-0.0961944	0.464902	-0.0962191
	0.3	0.484939	-0.0979956	0.449728	-0.0961419	0.457378	-0.0961817
	0.4	0.477725	-0.0980130	0.439322	-0.0960848	0.449728	-0.0961419
	0.5	0.470400	-0.0980315	0.428664	-0.0960224	0.441946	-0.0960995
3	0.1	0.694904	-0.0977065	0.674285	-0.0968360	0.675885	-0.0968387
	0.2	0.683143	-0.0977159	0.660527	-0.0968116	0.663790	-0.0968175
	0.3	0.671177	-0.0977260	0.646477	-0.0967851	0.651470	-0.0967947
	0.4	0.658993	-0.0977369	0.632115	-0.0967563	0.638914	-0.0967702
	0.5	0.646579	-0.0977486	0.617419	-0.0967248	0.626105	-0.0967437

TABLE II. Fundamental QNM frequencies for scalar and electromagnetic field perturbations with various l and ϵ^2 in Finslerian SdS black holes. The values are calculated using the sixth-order WKB approximation, and the parameters used in the calculation are $m = 0$, $r_e = 1$, and $r_c = 100$.

l	ϵ^2	Electromagnetic					
		Scalar		Axial		Polar	
		$\text{Re}(\omega_0)$	$\text{Im}(\omega_0)$	$\text{Re}(\omega_0)$	$\text{Im}(\omega_0)$	$\text{Re}(\omega_0)$	$\text{Im}(\omega_0)$
0	0.1	0.220886	-0.2016370
1	0.1	0.585645	-0.1955000	0.484278	-0.1849440	0.496275	-0.1852330
	0.2	0.585645	-0.1955000	0.471981	-0.1846320	0.496275	-0.1852330
	0.3	0.585645	-0.1955000	0.459364	-0.1842930	0.496275	-0.1852330
	0.4	0.585645	-0.1955000	0.446399	-0.1839250	0.496275	-0.1852330
	0.5	0.585645	-0.1955000	0.433056	-0.1835220	0.496275	-0.1852330
2	0.1	0.953816	-0.1935270	0.896307	-0.1898830	0.901011	-0.1899070
	0.2	0.940416	-0.1935600	0.877242	-0.1897790	0.886826	-0.1898320
	0.3	0.926823	-0.1935950	0.857754	-0.1896670	0.872410	-0.1897520
	0.4	0.913027	-0.1936320	0.837815	-0.1895440	0.857754	-0.1896670
	0.5	0.899020	-0.1936710	0.817392	-0.1894110	0.842844	-0.1895760
3	0.1	1.328280	-0.1929790	1.287690	-0.1911420	1.290750	-0.1911480
	0.2	1.305800	-0.1929990	1.261360	-0.1910900	1.267610	-0.1911030
	0.3	1.282920	-0.1930210	1.234470	-0.1910350	1.244030	-0.1910550
	0.4	1.259620	-0.1930440	1.206990	-0.1909740	1.220000	-0.1910030
	0.5	1.235890	-0.1930690	1.178860	-0.1909070	1.195480	-0.1909470

eigenvalues (13)–(14) that depend on the magnetic quantum number m . It will cause a Zeeman-like splitting of the QNM spectrum. The numerical results are shown graphically in Figs. 8–10, respectively. For scalar field perturbations, the

magnitude of $\text{Re}(\omega_0)$ decreases as m increases, while the magnitude of $|\text{Im}(\omega_0)|$ increases as m increases. For axial and polar modes of the electromagnetic field, the magnitudes of $\text{Re}(\omega_0)$ and $|\text{Im}(\omega_0)|$ are restrained with higher m .

TABLE III. Fundamental QNM frequencies for scalar field perturbations with various l and ϵ^2 in Finslerian RNdS black holes. The values are calculated using the sixth-order WKB approximation, and the parameters used in the calculation are $m = 0$, $b = 10^{-5}$, and $q = 0.5$.

l	ϵ^2	$\text{Re}(\omega_0)$	$\text{Im}(\omega_0)$
0	0.1	0.115752	-0.1019790
1	0.1	0.306506	-0.0988663
2	0.1	0.498989	-0.0979534
	0.2	0.491982	-0.0979689
	0.3	0.484874	-0.0979853
	0.4	0.477661	-0.0980028
	0.5	0.470336	-0.0980214
3	0.1	0.694815	-0.0976954
	0.2	0.683055	-0.0977048
	0.3	0.671090	-0.0977150
	0.4	0.658907	-0.0977258
	0.5	0.646495	-0.0977376

2. Prony method

In this section we use the Prony method [54] to calculate the frequencies of QNMs from the time-domain profile obtained using the finite difference method. Introducing a superposition of damped exponents,

$$\Psi(t) \approx \sum_{j=1}^p C_j e^{-i\omega_j t}, \quad (21)$$

the time-domain profile can be fitted. The time interval of the time-domain profile selected to fit begins at $t_0 = 0$ and ends at $t = Nh$, where N is an integer and satisfies $N \geq 2p - 1$. Using Eq. (21), the time-domain data can be expressed as

$$R(nh) \simeq \sum_{j=1}^p C_j e^{-i\omega_j nh} = \sum_{j=1}^p C_j z_j^n. \quad (22)$$

Thus, z_j can be obtained using the known $R(nh)$, and a polynomial function $A(z)$ designed to find z_j is defined as

$$A(z) = \prod_{j=1}^p (z - z_j) = \sum_{m=0}^p \alpha_m z^{p-m}, \quad \alpha_0 = 1. \quad (23)$$

Then, we can obtain the sum

$$\begin{aligned} \sum_{m=0}^p \alpha_m R_{n-m} &= \sum_{m=0}^p \alpha_m \sum_{j=1}^p C_j z_j^{n-m} \\ &= \sum_{j=1}^p C_j z_j^{n-p} A(z_j) = 0. \end{aligned} \quad (24)$$

Considering $\alpha_0 = 1$, we get the matrix equation

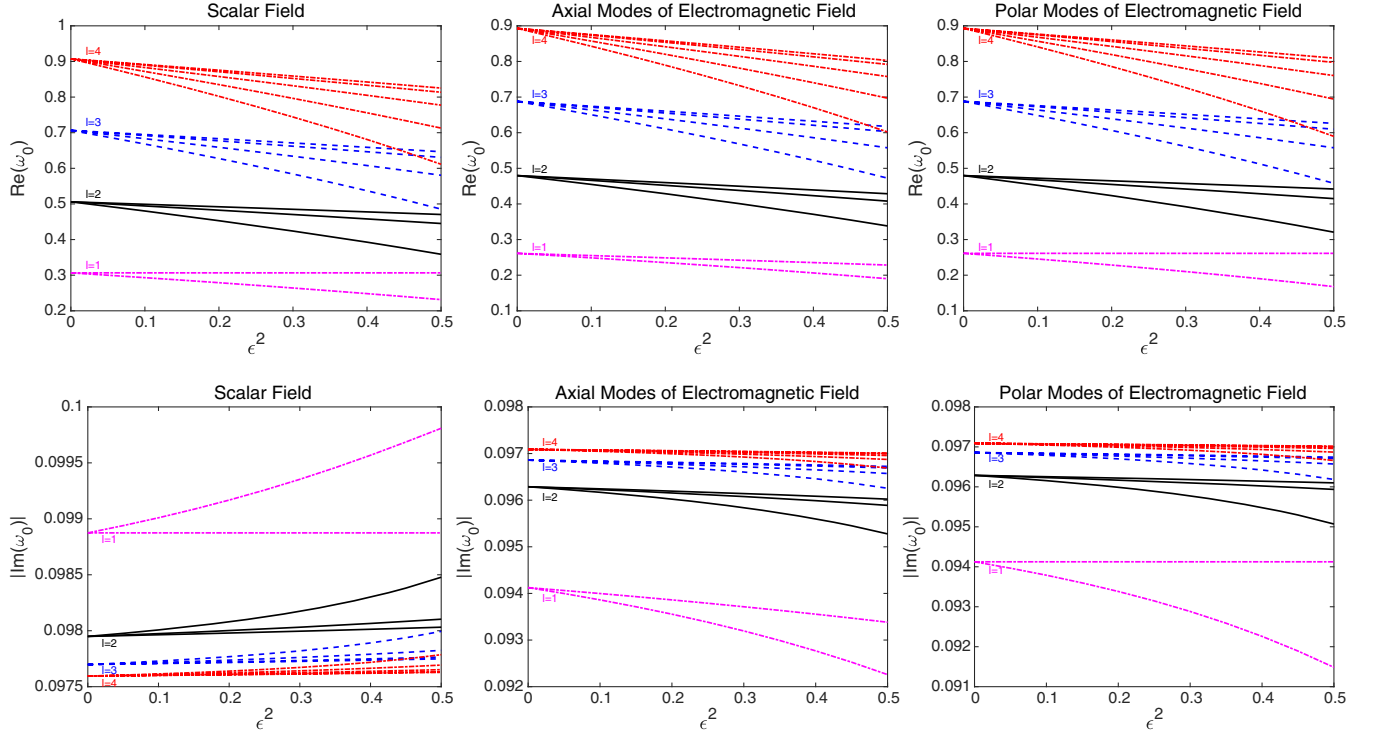


FIG. 8. Real and imaginary parts of the fundamental quasinormal frequencies of scalar and electromagnetic field perturbations in Finslerian RN black holes with $l = 1, 2, 3, 4$ and varying m . Lines refer to $m = 0, \dots, l$ from top to bottom for $\text{Re}(\omega_0)$, and from bottom to top for $|\text{Im}(\omega_0)|$ for scalar field perturbations. Lines refer to $m = 0, \dots, l$ from top to bottom for $\text{Re}(\omega_0)$ and $|\text{Im}(\omega_0)|$ for electromagnetic field perturbations.

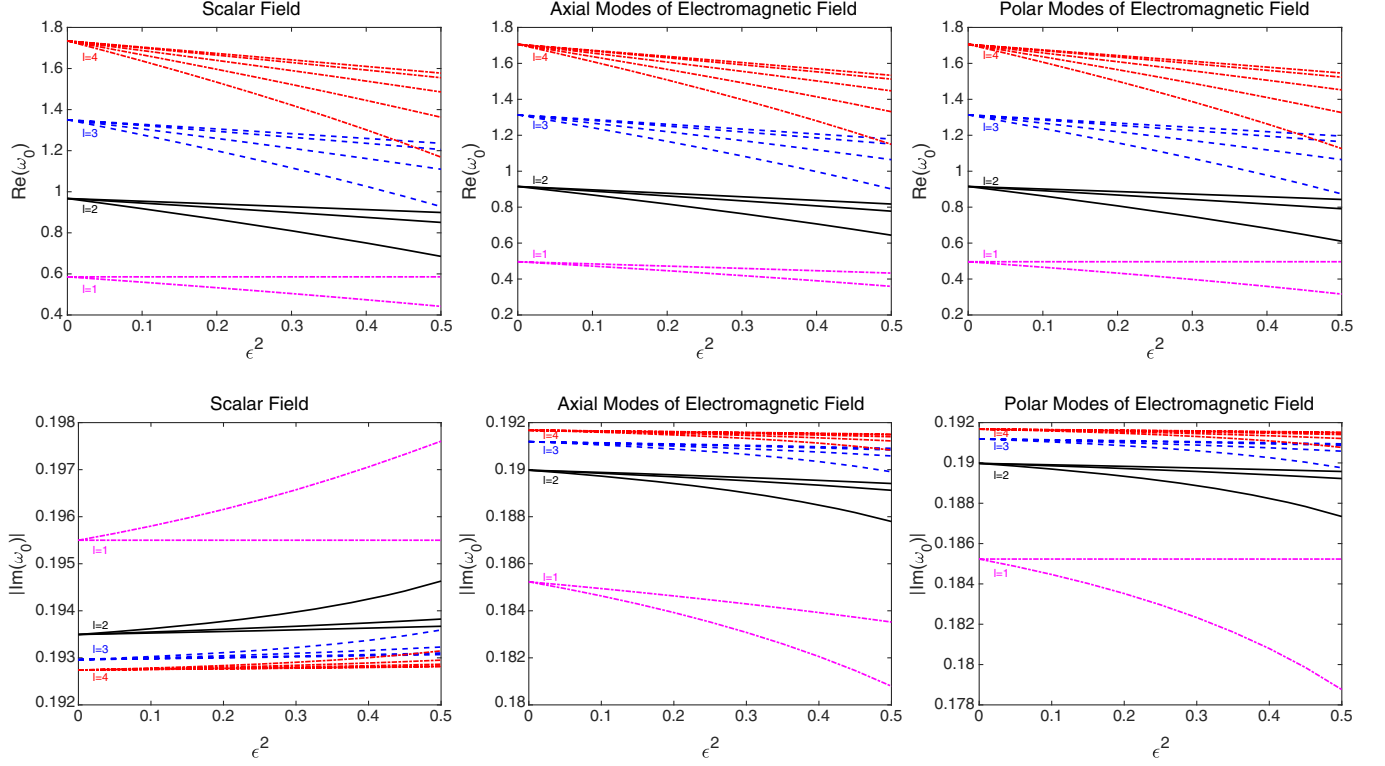


FIG. 9. Real and imaginary parts of the fundamental quasinormal frequencies of scalar and electromagnetic field perturbations in Finslerian SdS black holes with $l = 1, 2, 3, 4$ and varying m . Lines refer to $m = 0, \dots, l$ from top to bottom for $\text{Re}(\omega_0)$, and from bottom to top for $|\text{Im}(\omega_0)|$ for scalar field perturbations. Lines refer to $m = 0, \dots, l$ from top to bottom for $\text{Re}(\omega_0)$ and $|\text{Im}(\omega_0)|$ for electromagnetic field perturbations.

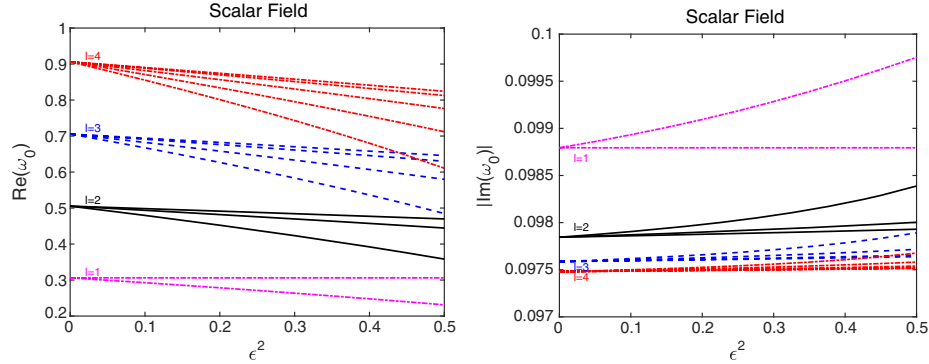


FIG. 10. Real and imaginary parts of the fundamental quasinormal frequencies of scalar field perturbations in Finslerian RNds black holes with $l = 1, 2, 3, 4$ and varying m . Lines refer to $m = 0, \dots, l$ from top to bottom for $\text{Re}(\omega_0)$, and from bottom to top for $|\text{Im}(\omega_0)|$.

$$\begin{pmatrix} R_{p-1} & R_{p-1} & \cdots & R_0 \\ R_p & R_{p-1} & \cdots & R_1 \\ \vdots & \vdots & \ddots & \vdots \\ R_{N-1} & R_{N-2} & \cdots & R_{N-p} \end{pmatrix} \begin{pmatrix} \alpha_1 \\ \vdots \\ \alpha_p \end{pmatrix} = - \begin{pmatrix} R_p \\ \vdots \\ R_N \end{pmatrix}.$$

By solving the above matrix equation and substituting it into $A(z)$, we can calculate z_j . With the relation $\omega_j = \frac{i}{h} \ln(z_j)$ we can obtain the frequencies of QNMs. The relative error

between the WKB approximation and Prony method is given by

$$\sigma = \left| 1 - \frac{\|\omega^{\text{Prony}}\|}{\|\omega^{\text{WKB}}\|} \right|. \quad (25)$$

Applying the Prony method to the time-domain profile calculated in Sec. III A, we get the fundamental frequencies with a relative error $\sigma < 0.001$. The comparisons of the frequencies obtained from the WKB approximation and

TABLE IV. Frequencies of the QNMs of scalar and electromagnetic field perturbations for Finslerian RN black holes with varying ϵ^2 . The parameters used are $(l, m) = (2, 0)$ and other parameters are the same as ones in the article.

Field	ϵ^2	ω^{WKB}	ω^{Prony}	σ
Scalar	0	$0.505966 - 0.0979492i$	$0.506153 - 0.0971758i$	7.25×10^{-5}
	0.4	$0.477725 - 0.0980130i$	$0.477808 - 0.0977648i$	6.46×10^{-5}
	0.7	$0.455396 - 0.0980724i$	$0.455243 - 0.0988687i$	3.93×10^{-5}
Axial	0	$0.479598 - 0.0962877i$	$0.479867 - 0.0950132i$	2.95×10^{-5}
	0.4	$0.439322 - 0.0960848i$	$0.439380 - 0.0958273i$	2.96×10^{-6}
	0.7	$0.406515 - 0.0958786i$	$0.406574 - 0.0956769i$	2.72×10^{-5}
Polar	0	$0.479598 - 0.0962877i$	$0.479867 - 0.0950132i$	2.95×10^{-5}
	0.4	$0.449728 - 0.0961419i$	$0.449421 - 0.0975668i$	6.20×10^{-7}
	0.7	$0.425958 - 0.0960058i$	$0.426043 - 0.0956346i$	2.64×10^{-6}

TABLE V. Frequencies of QNMs of scalar and electromagnetic field perturbations for Finslerian SdS black holes with varying ϵ^2 . The parameters used are $(l, m) = (2, 0)$ and other parameters are the same as ones in the article.

Field	ϵ^2	ω^{WKB}	ω^{Prony}	σ
Scalar	0	$0.967030 - 0.1934960i$	$0.968078 - 0.1887937i$	1.18×10^{-4}
	0.4	$0.913027 - 0.1936320i$	$0.913319 - 0.1922369i$	3.14×10^{-6}
	0.7	$0.870330 - 0.1937590i$	$0.870656 - 0.1922204i$	1.67×10^{-5}
Axial	0	$0.914977 - 0.1899780i$	$0.916250 - 0.1840692i$	6.94×10^{-5}
	0.4	$0.837815 - 0.1878535i$	$0.838172 - 0.1878535i$	2.66×10^{-5}
	0.7	$0.774941 - 0.1891020i$	$0.774913 - 0.1889345i$	8.44×10^{-5}
Polar	0	$0.914977 - 0.1899780i$	$0.916250 - 0.1840692i$	6.94×10^{-5}
	0.4	$0.857754 - 0.1896670i$	$0.859409 - 0.1824479i$	1.01×10^{-4}
	0.7	$0.812206 - 0.1893750i$	$0.813202 - 0.1854296i$	1.01×10^{-4}

TABLE VI. Frequencies of QNMs of scalar and electromagnetic field perturbations for Finslerian RNdS black holes with varying ϵ^2 . The parameters used are $(l, m) = (2, 0)$ and other parameters are the same as ones in the article.

Field	ϵ^2	ω^{WKB}	ω^{Prony}	σ
Scalar	0	$0.505899 - 0.0979388i$	$0.503321 - 0.1103802i$	1.97×10^{-5}
	0.4	$0.477661 - 0.0980028i$	$0.474498 - 0.1122827i$	1.80×10^{-5}
	0.7	$0.455335 - 0.0980624i$	$0.451813 - 0.1134557i$	1.40×10^{-4}

Prony method are shown in Tables IV and V for the scalar and electromagnetic field of Finslerian RN black holes and Finslerian SdS black holes, and in Table VI for the scalar field of Finslerian RNdS black holes, respectively. The results obtained using the Prony method show that the dynamical evolutions of scalar and electromagnetic field perturbations are consistent with the results obtained from the WKB approximation.

C. Late-time tails

In this section we focus on the behaviors of the late-time tails. The QNMs of black holes in general relativity are

suppressed by exponential or power-law tails at sufficiently late times [36]. The late-time tails of both SdS black holes and RNdS black holes exhibit an exponential falloff [41,47]. Our numerical investigations on the late-time tails of Finslerian SdS black holes and Finslerian RNdS black holes show that they follow the same behavior as that in SdS and RNdS black holes, respectively, and no major differences are found when the Finslerian parameter ϵ^2 ranges from 0 to 0.7. Thus, we will discuss the late-time tails of the Finslerian Schwarzschild black holes and Finslerian RN black holes.

A complete and generic approach to analyzing the late-time tails of QNMs was presented in Ref. [36]. There it was found that the behavior of the late-time tails depends on the

TABLE VII. Behaviors of late-time tails for Finslerian black holes.

Spacetime	Field	ϵ^2	$R(t \rightarrow +\infty)$
Finslerian Schwarzschild/Finslerian RN	Scalar/Electromagnetic	$\epsilon^2 = 0$	$t^{-(2\nu+3)}$
		$\epsilon^2 \neq 0$	$t^{-(2\nu+2)}$

TABLE VIII. Behaviors of late-time tails of scalar and electromagnetic field perturbations for Finslerian Schwarzschild black holes and Finslerian RN black holes. The values denote the power-law index, and common parameters are set as $l = 2$ and $m = 0$.

ϵ^2	Finslerian Schwarzschild			Finslerian RN		
	Scalar	Electromagnetic		Scalar	Electromagnetic	
		Axial	Polar		Axial	Polar
0	-7.04204	-7.04228	-7.04228	-7.04190	-7.04210	-7.04210
0.1	-5.89842	-5.89346	-5.89855	-5.89834	-5.89336	-5.89845
0.2	-5.86398	-5.82536	-5.86413	-5.86390	-5.82525	-5.86402
0.3	-5.80419	-5.73773	-5.80435	-5.80410	-5.73761	-5.80423
0.4	-5.73756	-5.64387	-5.73773	-5.73747	-5.64374	-5.73761
0.5	-5.66756	-5.54621	-5.66773	-5.66746	-5.54608	-5.66761

TABLE IX. Theoretical calculation of the behaviors of late-time tails of scalar and electromagnetic field perturbations for Finslerian Schwarzschild black holes and Finslerian RN black holes. The values denote the power-law index, and common parameters are set as $l = 2$ and $m = 0$.

ϵ^2	Scalar/Polar	Axial
0	-7.00000	-7.00000
0.1	-5.93095	-5.90772
0.2	-5.86092	-5.81368
0.3	-5.78988	-5.71774
0.4	-5.71774	-5.61984
0.5	-5.64450	-5.51980

specific form of the effective potential of the Schrödinger-like equation. In Finslerian Schwarzschild black holes and Finslerian RN black holes, the effective potentials (10), (11), and (12) all satisfy the following form

$$V(r_*) \approx \frac{\nu(\nu+1)}{r_*^2} + \frac{k_1}{r_*^3} \ln\left(\frac{r_*}{k_2}\right), \quad (26)$$

where $\nu(\nu+1) = \lambda^5$ corresponds to the scalar field and the polar mode of the electromagnetic field, $\nu(\nu+1) = \lambda^4$ corresponds to the axial mode of the electromagnetic field, and k_1 and k_2 are parameters related to the physical parameter GM and eigenvalues λ .

Following the analysis of Ref. [36], one can find that the parameter ν in Eq. (26) plays an important role in determining the behavior of the late-time tails. While ν is a noninteger, the first term in the potential, i.e., $\nu(\nu+1)/r_*^2$ (called the

centrifugal barrier) is dominant. Under such a condition, the radial and time components of field perturbations $R(r_*, t)$ behave as

$$R(r_*, t) \sim 2 \sin(\nu\pi) t^{-(2\nu+2)}, \quad (27)$$

when $r_* \rightarrow \infty$. The above formula tells us that the centrifugal barrier term does not contribute to the late-time tails if ν is an integer. Thus, the second term of Eq. (26) should be considered. Under such a condition, $R(r_*, t)$ behaves as

$$R(r_*, t) \sim t^{-(2\nu+3)} \quad (28)$$

when $r_* \rightarrow \infty$.

The behaviors of late-time tails are listed in Table VII for Finslerian black holes. One can find that the late-time tails of the QNMs of both Finslerian-Schwarzschild black holes and Finslerian RN black holes possess a power-law falloff.

In this paper we use the least-squares method to investigate the behaviors of the late-time tails of scalar and electromagnetic field perturbations for the considered black holes by analyzing the numerical results of the dynamic evolutions of QNMs. The numerical and theoretical results are shown in Tables VIII and IX, respectively. To find the differences of tails between Finslerian black holes and Riemannian black holes, we choose the fixed l and m in λ [Eqs. (13)–(14)] and only vary the values of the Finslerian parameter ϵ^2 . From Table VIII, we find that our numerical results are consistent with those of Schwarzschild black holes and RN black holes when $\epsilon^2 = 0$. Moreover, the numerical results are consistent with the theoretical results.

IV. DISCUSSION AND CONCLUSION

In this paper, we have studied the QNMs of Finslerian RN black holes with a cosmological constant. Two basic differences between such Finslerian black holes and its counterpart in general relativity, namely, two-dimensional subspace of the Finslerian black holes breaks spherical symmetry and asymptotic infinity of the Finslerian RN black holes without cosmological constant is not a Minkowski spacetime. The spectrum-splitting features of the QNMs of the Finslerian black holes were shown in Figs. 8–10. This reflects the spherical symmetry breaking. The late-time tails of the QNMs of both the Finslerian Schwarzschild black holes and Finslerian RN black holes possess a power-law falloff. The power-law index has a discontinuous jump, while the Finslerian parameter ϵ^2 varies from 0 to nonzero. Such a fact reflects that asymptotic infinity of the Finslerian black holes is not a Minkowski spacetime. It should be noticed that the Finslerian black holes will reduce to the counterparts black holes in general relativity while the Finslerian parameter $\epsilon^2 = 0$. Under this special condition, our numerical results on QNMs are consistent with those in general relativity [41,47–50].

The analysis of the dynamical evolution of QNMs shows that Finslerian RN black holes with a cosmological constant are stable under perturbations. Together with our former research [34], we found that the Finslerian black holes where their two-dimensional subspace is Finsler space with constant curvature are stable under perturbations. In this paper, we only considered the two-dimensional subspace of Finslerian black holes \bar{F} with the specific form (3). It should be noticed that Finsler spaces with constant curvature are not equivalent. It is expected that other two-dimensional subspaces, such as that derived by Byrant [38], will behave differently on the QNMs. Therefore, the frequencies of QNMs and the power-law index derived from the late-time tail will be useful tools to determine whether black holes are Finslerian or not and their deviation from spherical symmetry.

ACKNOWLEDGMENTS

This work has been supported by the National Natural Science Fund of China (Grants No. 11775038 and No. 12147102).

-
- [1] R. Penrose, *Phys. Rev. Lett.* **14**, 57 (1965).
 - [2] A. Celotti, J. C. Miller, and D. W. Sciama, *Classical Quantum Gravity* **16**, A3 (1999).
 - [3] B. J. Carr and S. W. Hawking, *Mon. Not. R. Astron. Soc.* **168**, 399 (1974).
 - [4] A. D. Dolgov and S. I. Blinnikov, *Phys. Rev. D* **89**, 021301 (R) (2014).
 - [5] S. Clesse and J. Garcia-Bellido, *Phys. Rev. D* **92**, 023524 (2015).
 - [6] S. B. Giddings and S. Thomas, *Phys. Rev. D* **65**, 056010 (2002).
 - [7] J. A. Munoz, E. Mediavilla, C. S. Kochanek, E. E. Falco, and A. M. Mosquera, *Astrophys. J.* **742**, 67 (2011).
 - [8] F. Yuan and R. Narayan, *Annu. Rev. Astron. Astrophys.* **52**, 529 (2014).
 - [9] R. Abuter *et al.* (the Gravity Collaboration), *Astron. Astrophys.* **625**, L10 (2019).
 - [10] K. Akiyama *et al.* (the Event Horizon Telescope Collaboration), *Astrophys. J. Lett.* **875**, L6 (2019).
 - [11] B. P. Abbott *et al.* (LIGO Scientific and Virgo Collaborations), *Phys. Rev. X* **9**, 031040 (2019).
 - [12] B. Sathyaprakash *et al.*, *Classical Quantum Gravity* **29**, 124013 (2012).
 - [13] C. M. Will, *Living Rev. Relativity* **17**, 4 (2014); **4**, 4 (2001).
 - [14] T. Clifton, P. G. Ferreira, A. Padilla, and C. Skordis, *Phys. Rep.* **513**, 1 (2012).
 - [15] T. P. Sotiriou and V. Faraoni, *Rev. Mod. Phys.* **82**, 451 (2010).
 - [16] T. Harko, F. S. N. Lobo, S. Nojiri, and S. D. Odintsov, *Phys. Rev. D* **84**, 024020 (2011).
 - [17] J. D. Bekenstein, *Phys. Rev. D* **70**, 083509 (2004).
 - [18] D. Bao, S. S. Chern, and Z. Shen, *An Introduction to Riemann-Finsler Geometry* (Springer Press, New York, 2000), pp. 1–96.
 - [19] S. F. Rutz, *Gen. Relativ. Gravit.* **25**, 1139 (1993).
 - [20] X. Li and Z. Chang, *Phys. Rev. D* **90**, 064049 (2014).
 - [21] X. Li, *Phys. Rev. D* **98**, 084030 (2018).
 - [22] E. Minguzzi, *Living Rev. Relativity* **22**, 3 (2019); A. B. Aazami and M. A. Javaloyes, *Classical Quantum Gravity* **33**, 025003 (2016).
 - [23] E. Berti *et al.*, *Classical Quantum Gravity* **32**, 243001 (2015).
 - [24] E. Berti, V. Cardoso, and A. O. Starinets, *Classical Quantum Gravity* **26**, 163001 (2009).
 - [25] R. A. Konoplya and A. Zhidenko, *Rev. Mod. Phys.* **83**, 793 (2011).
 - [26] S. Chakraborty, K. Chakravarti, S. Bose, and S. SenGupta, *Phys. Rev. D* **97**, 104053 (2018).
 - [27] C. Molina, A. B. Pavan, and T. E. Medina Torrejon, *Phys. Rev. D* **93**, 124068 (2016).
 - [28] J. L. Blazquez-Salcedo, D. D. Doneva, J. Kunz, K. V. Staykov, and S. S. Yazadjiev, *Phys. Rev. D* **98**, 104047 (2018).
 - [29] O. J. Tattersall and P. G. Ferreira, *Phys. Rev. D* **97**, 104047 (2018).
 - [30] S. Datta and S. Bose, *Eur. Phys. J. C* **80**, 14 (2020).

- [31] R. Abbott *et al.* (LIGO Scientific, Virgo, and KAGRA Collaborations), *Astrophys. J. Lett.* **915**, L5 (2021).
- [32] P. Amaro-Seoane *et al.*, [arXiv:1702.00786](https://arxiv.org/abs/1702.00786).
- [33] W.-H. Ruan, C. Liu, Z.-K. Guo, Y.-L. Wu, and R.-G. Cai, *Research* **2021**, 6014164 (2021).
- [34] X. Li and S.-P. Zhao, *Phys. Rev. D* **101**, 124012 (2020).
- [35] Planck Collaboration, *Astron. Astrophys.* **594**, A13 (2016).
- [36] E. S. C. Ching, P. T. Leung, W. M. Suen, and K. Young, *Phys. Rev. D* **52**, 2118 (1995); *Phys. Rev. Lett.* **74**, 2414 (1995).
- [37] M. A. Javaloyes and M. Sanch, *Rev. R. Acad. Cienc. Exactas Fis. Nat. Ser. A Mat.* **114**, 30 (2020).
- [38] R. L. Bryant, *Sel. Math. New Ser.* **3**, 161 (1997).
- [39] Z. Shen, *Manuscr. Math.* **109**, 349 (2002).
- [40] F. Mellor and I. Moss, *Phys. Rev. D* **41**, 403 (1990).
- [41] C. Molina, D. Giugno, E. Abdalla, and A. Saa, *Phys. Rev. D* **69**, 104013 (2004).
- [42] T. Barthelme, *Isr. J. Math.* **196**, 375 (2013).
- [43] X. Mo and Y. Yang, *Sci. China, Ser. A Math. phys. astron. technol. sci.* **48A**, 115 (2005).
- [44] Z. Shen, *Lectures on Finsler Geometry* (World Scientific, Singapore, 2001).
- [45] Q. He, F.-Q. Zeng, and D.-X. Zheng, *Acta Math. Sci.* **37B**, 1162 (2017).
- [46] C. Gundlach, R. H. Price, and J. Pullin, *Phys. Rev. D* **49**, 883 (1994); **49**, 890 (1994).
- [47] P. R. Brady, C. M. Chambers, W. G. Laarakkers, and E. Poisson, *Phys. Rev. D* **60**, 064003 (1999).
- [48] B. F. Schutz and C. M. Will, *Astrophys. J.* **291**, L33 (1985).
- [49] S. Iyer and C. M. Will, *Phys. Rev. D* **35**, 3621 (1987); S. Iyer, *Phys. Rev. D* **35**, 3632 (1987).
- [50] R. A. Konoplya, *Phys. Rev. D* **68**, 024018 (2003).
- [51] R. A. Konoplya, *Phys. Rev. D* **66**, 084007 (2002).
- [52] K. Lin and W.-L. Qian, *Classical Quantum Gravity* **34**, 095004 (2017).
- [53] Y. Zhang, E.-K. Li, and J.-L. Geng, *Gen. Relativ. Gravit.* **46**, 1728 (2014).
- [54] E. Berti, V. Cardoso, J. A. González, and U. Sperhake, *Phys. Rev. D* **75**, 124017 (2007).